Neuron
Article

The Ubiquitin Ligase Phr1 Regulates Axon Outgrowth through Modulation of Microtubule Dynamics

Joseph W. Lewcock,[1,2] Nicolas Genoud,[1] Karen Lettieri,[1] and Samuel L. Pfaff[1,*]
[1]Gene Expression Laboratory, The Salk Institute for Biological Studies, La Jolla, CA 92037, USA
[2]Present address: Neurobiology, Genentech, Inc., 1 DNA Way, South San Francisco, CA 94080, USA.
*Correspondence: pfaff@salk.edu
DOI 10.1016/j.neuron.2007.09.009

SUMMARY

To discover new genes involved in axon navigation, we conducted a forward genetic screen for recessive alleles affecting motor neuron pathfinding in GFP reporter mice mutagenized with ENU. In *Magellan* mutant embryos, motor axons were error prone and wandered inefficiently at choice points within embryos, but paradoxically responded to guidance cues with normal sensitivity in vitro. We mapped the *Magellan* mutation to the *Phr1* gene encoding a large multidomain E3 ubiquitin ligase. Phr1 is associated with the microtubule cytoskeleton within neurons and selectively localizes to axons but is excluded from growth cones. Motor and sensory neurons from *Magellan* mutants display abnormal morphologies due to a breakdown in the polarized distribution of components that segregate between axons and growth cones. The *Magellan* phenotype can be reversed by stabilizing microtubules with taxol or inhibiting p38MAPK activity. Thus, efficacious pathfinding requires Phr1 activity for coordinating the cytoskeletal organization that distinguishes axons from growth cones.

INTRODUCTION

Patterned neuronal connections are established through the directed growth of nascent axons toward their appropriate postsynaptic targets. This wiring process can be mediated by growth of the primary axon directly to the target or by delayed formation of interstitial axon branches that mediate target selection (McLaughlin and O'Leary, 2005). In both cases, however, the extension of neurites relies on the formation of a motile growth cone rich in filamentous (F) actin coated with membrane-linked receptors for monitoring the extracellular environment. The asymmetric activation of receptors on the growth cone surface initiates localized signaling that promotes either assembly or disassembly of the cytoskeleton on a subcellular scale, thereby leading to axon turning and highly specific navigation (Dickson, 2002; Van Vactor, 1998). This cellular model of wiring implies that embryonic neurons that grow to different targets (1) will each express unique constellations of signaling components (Tessier-Lavigne and Goodman, 1996) and (2) form coherent growth cones that maintain a polarized proximodistal orientation as they grow, so that guidance signals can be perceived at a subcellular level (Dent and Gertler, 2003). By defining the molecular components responsible for axon navigation and characterizing how these signals modulate cytoskeletal dynamics within the growth cone, it is anticipated that a better understanding of the general principles controlling neural circuit formation will emerge.

Many of the fundamental cellular and molecular features of axon pathfinding have come from studies of embryonic motor neurons (Landmesser, 1980). The development of these neurons occurs in a stepwise fashion in which homeodomain and basic helix-loop-helix transcription factors first establish a generic motor neuron identity, followed by further subtype specification through the combinatorial activity of LIM-homeodomain and Hox-class transcription factors (Briscoe and Ericson, 2001; Dasen et al., 2005; Jessell and Sanes, 2000; Shirasaki and Pfaff, 2002). Combinatorial transcription factor expression also appears to designate the projection targets of distinct motor neuron subtypes within the embryo (Dasen et al., 2005; Sharma et al., 2000). Downstream of these factors, several archetypal axon guidance pathways are thought to directly influence the process of motor axon navigation. For example, Sema3A regulates the fasciculation and timing of motor axon outgrowth through Npn-1 receptors (Huber et al., 2005; Varela-Echavarria et al., 1997), and EphA4 directs dorsal-ventral projection decisions into the limb (Eberhart et al., 2002; Helmbacher et al., 2000; Kania and Jessell, 2003). In addition, several unconventional motor axon guidance signaling pathways have been identified, such as the chemokine Cxcl12 (via the Cxcr4 receptor) for motor axon exit from the neural tube (Lieberam et al., 2005), the neurotrophin GDNF (via cRet), and ephrin-A5 reverse signaling for dorsal limb innervation (Kramer et al., 2006; Marquardt et al., 2005), the growth factor FGF (via FGFR1) for axial muscle

targeting (Shirasaki et al., 2006), and the growth factor HGF (via cMet) for various projections (Ebens et al., 1996). Once motor axons reach their muscle targets, growth factors such as GDNF have additional roles in promoting axonal arborization and dendrite development (Haase et al., 2002; Helmbacher et al., 2003; Vrieseling and Arber, 2006), while BDNF and HGF have been shown to promote motor neuron survival and axon branching in vitro (Helmbacher et al., 2003; Novak et al., 2000; Ozdinler and Macklis, 2006; Yamamoto et al., 1997). Despite these discoveries, our understanding of this complex developmental process is still somewhat fragmentary, and a more comprehensive understanding of the molecular and temporal regulation of these developmental steps is required to understand how the intricate pattern of motor innervation is established.

Forward genetic screens in *Drosophila* and *C. elegans* have proven effective for the identification of molecules involved in neuronal development and connectivity (Callahan et al., 1995; Finney et al., 1988; Kolodkin et al., 1993; Zallen et al., 1998). We reasoned that, if motor neurons and their axons could be visualized at high resolution in vivo, forward genetics in mice would be a powerful unbiased approach for identification of factors governing their development. To do this, we generated transgenic mice that expressed a membrane-localized GFP specifically in motor neurons and then incorporated this line into an ENU mutagenesis screen for recessive alleles affecting motor axon navigation. Six highly penetrant and phenotypically unique mutant lines were isolated in the screen, and here we focus on the *Magellan* line that exhibits motor axon misprojections and stalling. The *Magellan* mutation was mapped to a premature stop codon in the *Phr1* gene (*PAM*, *Highwire*, and *RPM-1*), which encodes a large approximately 4700 aa multidomain protein with potential leucine zipper motifs, homology to guanine exchange factors (GEFs), a myc interaction domain, and a C-terminal zinc finger RING-H2 domain typical of E3-ubiquitin ligases (Burgess et al., 2004; Guo et al., 1998). Genetic studies in *Drosophila* and *C. elegans* have found that *Phr1* homologs *hiw* and *rpm-1*, respectively, are necessary for proper synapse formation (Schaefer et al., 2000; Wan et al., 2000; Zhen et al., 2000). The piebald deletion in mice that eliminates *Phr1*, *Scel*, and the novel transcript *TC255155* results in excessive nerve terminal sprouting (Burgess et al., 2004), but defects in neuronal morphology make it unclear whether synaptic defects arise secondarily. In zebrafish *esrom* mutants (*Phr1* ortholog), retinal axons terminate at inappropriate tectal positions, presumably due to premature arborization, yet the overall degree of axonal branching in vivo is not altered (D'Souza et al., 2005). Although *Phr1* represents an evolutionarily conserved gene required for neuronal development, its mechanism of function in axon guidance remains poorly understood.

In this study, we demonstrate that Phr1 is tightly associated with the microtubule cytoskeleton and is enriched in axons but not their growth cones. Explants from *Phr1* mutants exhibited normal rates of neurite growth and responded properly to both attractive and repulsive guidance cues, but had defective growth cones that caused neurites to wander inappropriately during growth. These defects were attributed to aberrant microtubule dynamics, which resulted in an inability of axons to properly define the distinction between the dynamic growth cone and stable axon shaft. The severity of these defects could be reduced through treating mutant axons with a chemical inhibitor of P38MAPK or the microtubule stabilizer taxol, implying that Phr1 participates in MAPK signaling pathways that function to regulate mircotubule stability on a subaxonal level. Taken together, the synaptic defects, axon branching phenotypes, and misprojections observed in different *Phr1*/*Hiw*/*RPM-1* mutant contexts suggest that several distinct aspects of neuronal development may be linked by virtue of sharing common signaling components that regulate cytoskeletal organization.

RESULTS

A Forward Genetic Screen for Embryonic Motor Defects

In order to identify genes underlying the proper development of the spinal motor system, we employed a mouse mutagenesis screen based on a strategy first used to identify recessive patterning mutations (Kasarskis et al., 1998). The design of our screen included a novel transgenic GFP reporter that selectively labels all spinal motor neurons in order to facilitate identification of recessive motor defects (Figure 1A). The transgene used to label motor neurons was constructed by fusing a motor neuron enhancer from the *Isl1* gene to a GFP tagged with the Ras farnysylation sequence for membrane localization (ISL^{MN}*:GFP*, Figure 1B). ISL^{MN}*:GFP* embryos express GFP in all somatic motor neurons, with particularly high expression in the MMCm and slightly lower levels in other motor columns that project to the body wall and limbs (Figure 1C). Single motor axons were visible in whole-mount preparations of embryonic day 12.5 (E12.5) embryos from this transgenic line, providing an excellent comprehensive view of motor axon projections during their development (Figure 1D).

3383 embryos derived from backcrosses of 88 F1 families each estimated to have ~2500 point mutations (Concepcion et al., 2004) were dissected and flat-mounted at E12.5 to visualize GFP-labeled motor axons. Mutant embryos were identified based on the presence of one or more of the following defects: abnormal motor axon outgrowth, axon stalling, misguided axon projections, altered motor neuron cell numbers, or inappropriate cell body positions. Motor neuron defects found in embryos with overt morphological phenotypes were discarded to minimize characterization of indirect developmental processes. From this screen, six mutant lines were identified with reproducible motor neuron phenotypes appearing in litters at Mendelian ratios. The mutants were named after navigators of the European colonial period and exhibited an assortment of motor axon navigation defects

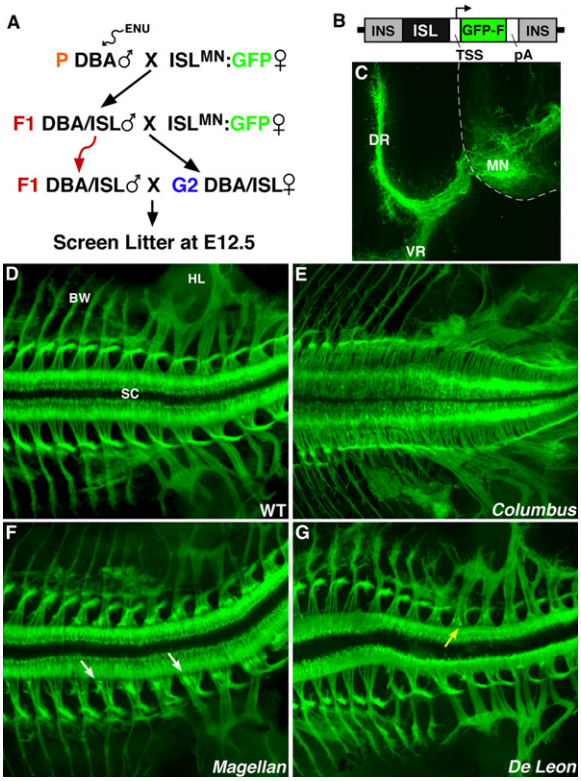

Figure 1. ENU Screen for Recessive Alleles Affecting Spinal Motor Neurons

(A) Diagram of ENU screening strategy. Male DBA mice were mutagenized with ENU and mated for two generations to *ISL^{MN}:GFP* mice. G2 females were mated to F1 males in the same family, and litters were screened at E12.5 for motor neuron defects.

(B) The *ISL^{MN}:GFP* construct used to label motor neurons consists of a farnesylated GFP driven by a motor neuron enhancer from the ISL1 gene linked to a minimal promoter and flanked by insulator sequences.

(C) Transverse section of a normal E12.5 *ISL^{MN}:GFP* embryo. GFP labels motor neuron cell bodies within the cord (MN), motor axons within the dorsal ramus (DR) projecting to back muscles, and the ventral ramus (VR) to body wall or limb muscles.

(D) Flat-mount image of an E12.5 *ISL^{MN}:GFP* embryo. Motor columns can be visualized in the spinal cord (SC), as well as motor projections to the body wall (BW) and hindlimb (HL).

(E) *Columbus* mutants display abnormal motor column organization and multiple axon navigation defects, including the loss of discrete ventral roots.

(F) *Magellan* mutants exhibit highly fluorescent GFP puncta (arrows) close to the spinal cord at lower thoracic and lumbar levels.

(G) *De Leon* mutants also display GFP^{+} puncta in the ventral root (arrow) and reduced projections to the dermomyotome.

(Table 1). For example, *Columbus* mutant embryos displayed improper motor column formation, and their motor axons failed to form discrete ventral roots as they exited the spinal cord (Figure 1E). In contrast, motor projections in *De Leon* mutant embryos were largely normal, although a subset of lumbar axons appeared to project aberrantly shortly after exiting the spinal cord (Figure 1G). A third line, *Magellan*, displayed more severe projection errors in the ventral root, characterized by the presence of highly fluorescent GFP puncta at thoracic and lumbar levels with 100% penetrance (Figure 1F). Despite extensive errors in motor axon projections, mutant embryos from most lines could not be distinguished from their wild-type littermates and were only apparent because of the *ISL^{MN}:GFP* reporter.

Table 1. Mutations that Cause Specific Spinal Motor Defects

Mutant	Phenotype	Map Position Chr:cM	Gene
Magellan	GFP+ puncta in ventral roots, limb innervation defects	14: 57	Phr1
Columbus	No discrete ventral roots, many projection errors	12: 33	
De Leon	Aberrantly projecting axons close to spinal cord	6: 51	Cxcr4
Cortes	Abnormal motor column formation at lumbar levels	11:3–10	
Pizarro	Misprojecting axons specifically at thoracic levels	12: 10–30	
Vespucci	Severe axon guidance defects proximal to spinal cord	**	
Mag^{sp}	GFP+ puncta in ventral roots, limb innervation defects	14: 57	Phr1

**Mapping complicated due to incompletely penetrant dominant phenotype.

Phr1 Is Truncated in *Magellan* Mutants

The *Magellan* line was selected for examination in more detail because mutant embryos displayed severe motor defects dissimilar to any previously observed phenotype. The mutation was mapped to an ~5 Mb segment on the distal end of chromosome 14 in a region that contains few predicted protein-coding genes (*Ensembl* database). *Phr1* was identified as a candidate gene responsible for the *Magellan* phenotype within this segment due to the neuronal-specific expression and activity of its orthologs *highwire* (Wan et al., 2000), *rpm-1* (Zhen et al., 2000), and *esrom* (D'Souza et al., 2005), as well as the diaphragm innervation defects in mice with a chromosomal deletion that spans the *Phr1* locus (Burgess et al., 2004). To examine the possibility that the axon guidance defects observed in *Magellan* mutants resulted from a mutation in *Phr1*, the 14.5 kb cDNA was amplified from mutant and wild-type whole-embryo RNA and sequenced. This method was employed as an alternative to sequencing genomic DNA, because the *Phr1* gene contains 86 exons and

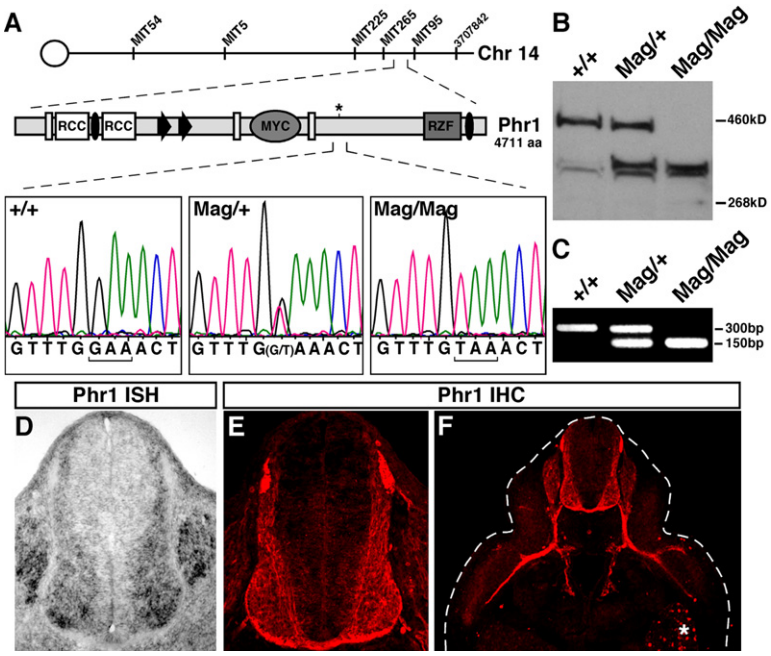

Figure 2. *Phr1* Has a Premature Stop Codon in the *Magellan* Mutant

(A) Schematic of the *Phr1* gene. *Magellan* was mapped to *Phr1*, a gene on the distal end of chromosome 14, using the MIT markers shown and others. *Phr1* encodes a large protein with a predicted size of ~4700 amino acids and contains multiple domains, including two Regulation of Chromatin Condensation (RCC) domains, two Phr domains (black arrows), a Myc binding domain (MYC), and a Ring zinc finger domain (RZF). The *Magellan* mutation (asterisk), identified as a G→T base transition in exon 63, generated a premature stop codon.

(B) Western blot analysis of Phr1 protein using an antibody directed to the N terminus detected a truncated protein in *Magellan* mutants. Heterozygous littermates expressed both the truncated and wild-type proteins.

(C) Restriction digest of a genomic PCR product that contains the *Magellan* mutation. The point mutation resulted in the generation of an *Hpy8I* recognition sequence not present in the wild-type sequence, cutting the DNA in half.

(D) In situ hybridization of E11.5 spinal cord with a probe for *Phr1*. It is expressed in motor neurons as well as other cell types in the spinal cord and DRG, but is absent from cells within the ventricular zone and periphery.

(E) Immunohistochemistry detects Phr1 protein in postmitotic neurons at E11.5.

(F) Low-magnification view of (E) showing neuronal specificity of Phr1 and labeling of motor and sensory axons. Asterisk indicates a small population of nonneuronal cells that transiently express Phr1 at this age.

spans >200 kb. Although full-length *Phr1* mRNA was present in mutant embryos, a G→T base transition was identified in the 63rd exon, which resulted in a premature termination codon (Figure 2A). The presence of this base conversion in genomic DNA of *Magellan* mutant embryos was also confirmed. All mutant embryos ($n > 25$) were homozygous for the G→T conversion, while no adult animals or phenotypically normal littermates were homozygous mutants ($n > 100$, Figure 2C).

We next investigated the effect of the *Magellan* mutation on levels of Phr1 protein using western blotting and found that the premature termination codon disrupted full-length Phr1 expression. Instead, a truncated form of Phr1 was detected in mutant embryos using an antibody generated against the N terminus (Santos et al., 2006) (Figure 2B). Members of the *Phr1* family are highly conserved in domain structure, and the mutation identified in the *Magellan* line eliminates the evolutionarily conserved C-terminal RING zinc finger domain that is required for proper function of Phr1 orthologs in flies, worms, and fish (D'Souza et al., 2005; Nakata et al., 2005; Wu et al., 2005).

During continued screening, an independent mutant was identified that displayed motor axon guidance defects similar to those observed in *Magellan*, and genetic mapping placed the mutation in the same region of chromosome 14 where *Phr1* resides (Table 1). To test whether this mutant represented a second *Magellan* allele, we crossed the two lines to generate embryos heterozygous for both mutations. Compound heterozygous embryos displayed a phenotype nearly identical to the original *Magellan* mutants (Figures 3A–3C), indicating this mutation likely also affected Phr1 activity. The second *Magellan* allele (designated *Magellan - splicing defective*, or Mag^{SP}) originated from a different ENU-treated male and therefore was predicted to contain a different mutation from the original *Magellan* line. This was confirmed through analysis of *Phr1* mRNA from E12.5 Mag^{SP} mutant embryos, which identified a 32 base deletion in exon 65 that caused a frameshift and a premature termination codon early in exon 66 (Figures 3D and 3E). Sequencing of the genomic DNA encoding exon 65 revealed that a G→A base conversion had generated a new splice donor in Mag^{SP} mutants that was responsible for the observed truncation. The discovery of a separate *Phr1* mutant allele provides additional evidence that disruption of Phr1 function causes the *Magellan* motor axon guidance phenotype.

Phr1 Expression in the Developing Spinal Cord

To determine whether Phr1 was likely to function in neurons, peripheral cells, or both, we first analyzed the expression of *Phr1* using in situ hybridization and immunohistochemistry. At E10.5, shortly after the birth of the first motor neurons, high levels of *Phr1* expression could be visualized in the developing motor columns, DRG, and newly formed neurons within the dorsal neural tube (see Figures S1A and S1B in the Supplemental Data available with this article online). As embryos developed to E11.5, *Phr1* expression levels increased in the DRG, and expression in the spinal cord expanded as the number of postmitotic neurons increased (Figures 2D and 2E). By E12.5,

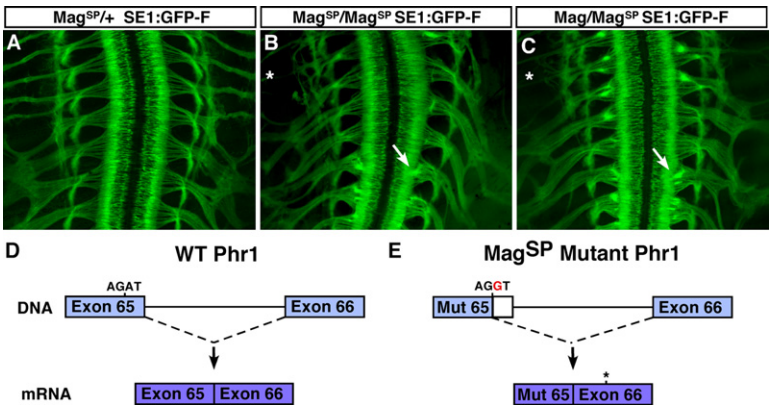

Figure 3. Identification of a Second Independent Mutation in *Phr1*

(A–C) Whole-mount view of *Mag*^{sp} mutant and *Magellan*/*Mag*^{sp} compound heterozygous embryos at E12.5. *Mag*^{sp} mutant embryos (B) display motor axon stalling similar to *Magellan* mutants (arrow) and have thinner intercostal nerves (asterisk). *Magellan*/*Mag*^{sp} compound heterozygous (C) exhibit an identical phenotype. This demonstrates that both mutations affect the same gene.

(D and E) Diagram of the *Mag*^{sp} mutation. While *Phr1* exons 65 and 66 were found in all wild-type samples examined (D), in *Mag*^{sp} mutants an A→G mutation results in the generation of a new splice donor in exon 65, a frameshift, and a termination codon early in exon 66 (asterisk).

Phr1 expression was widespread within the spinal cord, encompassing the Isl1/2^{+} motor neuron population (Figures S1C–S1E). Phr1 protein was restricted to the nervous system and included expression in motor and sensory axons (Figure 2F), although a subgroup of liver cells also appeared to be labeled. Thus, the expression of Phr1 suggests that it functions in neurons, as is the case with the invertebrate homologs *hiw* and *rpm-1* (Wan et al., 2000; Wu et al., 2005; Zhen et al., 2000).

Magellan Mutants Exhibit Defects in Motor and Sensory Innervation

We first focused on characterization of the motor projection errors proximal to the spinal cord, which varied slightly depending on the rostrocaudal level of the embryo. Axons at brachial segments (lower cervical) frequently misprojected dorsally from the ventral root and often inappropriately entered the dorsal root ganglion (DRG), while axons at lumbar levels appeared to wander or stall inappropriately within 100 μm of exiting the spinal cord (Figures 4A–4D). At upper thoracic levels, the stalling and misprojection phenotypes were both observed. Many of the growth defects and apparent stalling occurred at the major choice point where motor axons originating in the MMCm break from the ventral root and turn dorsally to innervate the dermomyotome (Figures 5G and 5H). The thickness of the intercostal nerves in *Magellan* mutants was also reduced compared to littermate controls (compare brackets in Figure 4C to 4D). This reduction in labeling probably arises from a decrease in the number of intercostal axons present in the nerve, as motor neuron numbers and subtype identity as assessed by nuclear marker profiles are normal in *Magellan* mutants (Figure S2, see below).

To determine whether additional motor projection decisions were affected in the *Magellan* mutants, we examined innervation of the hindlimb. Plexi located at the base of the limbs represent well-defined choice points where motor axons from multiple spinal cord levels converge before separating in a highly coordinated fashion to innervate the limb musculature (Landmesser, 1978). *Magellan* mutant embryos displayed severe projection defects at the crural plexus where the majority of motor axons failed to grow distally beyond this choice point, leading to reduced limb innervation (Figures 4E and 4F). Stalling was also observed at later developmental stages, indicating that this defect was not simply a temporal delay in limb innervation (data not shown). Taken together, many classes of motor neurons exhibited axon growth and pathfinding defects in *Magellan* mutants, and errors seemed to be most prevalent at major axonal choice points.

Although our screen was designed to identify defects in motor innervation, expression analyses confirmed that *Phr1* was broadly expressed in the developing CNS. We next examined whether peripheral sensory projections originating from the DRG were similarly affected by the *Magellan* mutation. Examination of cutaneous sensory innervation in *Magellan* mutants at E12.5 using whole-mount neurofilament staining revealed multiple errors in sensory innervation (Figures 4G and 4H). Axons appeared overgrown and sensory nerves were defasciculated (Figures 4I and 4J). As observed with the intercostal motor axons, this pattern of innervation resulted in thinner nerves at more distal locations (compare brackets in Figure 4I to 4J). The distal reduction in motor and sensory nerve size is consistent with individual axons straying from the nerve or stalling at proximal locations, leading to fewer axons at distal sites.

Motor Axons Wander and Turn Inappropriately at Choice Points in Magellan Mutants

To evaluate whether the innervation defects observed in *Magellan* mutants arose from axon navigation errors, we used the *ISL*^{MN}*:GFP* reporter to visualize motor axons as they navigate through the first choice point in the periphery. In wild-type embryos, a coherent ventral ramus has formed at E10.5, and a subset of thoracic motor axons defasciculate from this path and begin to turn dorsally toward the precursor of the axial (back) musculature, the dermomyotome, initiating the formation of the dorsal ramus nerve (Figure 5A, DR). In contrast, motor axons appear more disorganized at this choice point in *Magellan* mutants. Furthermore, the ventral ramus appeared reduced in size whereas a more prominent dorsal ramus projection was apparent (Figure 5B, asterisk).

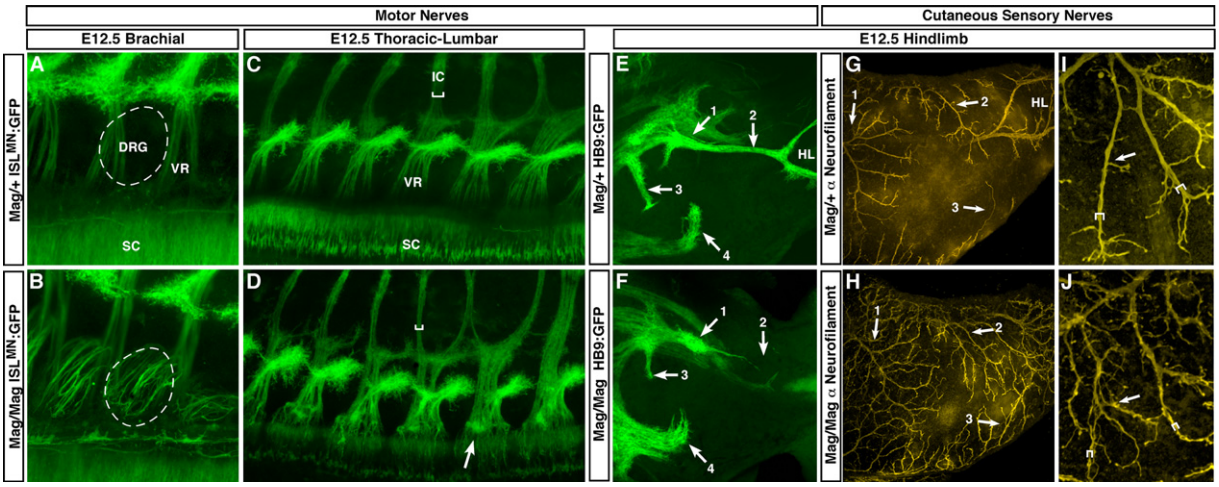

Figure 4. *Magellan* Mutants Display Numerous Motor and Sensory Innervation Defects

(A–D) Dorsal flat-mount view of motor axons exiting the spinal cord (SC) in E12.5 mice with the *ISL^{MN}:GFP* reporter. (A) Control. (B) A subset of brachial GFP^{+} motor axons in *Magellan* mutants separate from the ventral root (VR) and project inappropriately toward DRGs (one DRG traced with dashed circle). (C) At thoracic-lumbar levels, motor axons in control embryos project to the body wall (intercostal nerves, IC) and limb (not shown) or turn to innervate back musculature. (D) In *Magellan* mutants, the ventral roots are disorganized, and the thickness of the intercostal nerves is reduced (brackets).

(E and F) Motor projections in the hindlimb, visualized at E12.5 by crossing to *HB9:GFP* reporter mice. The majority of limb-projecting axons are stalled at the plexus in *Magellan* mutant embryos (arrow 1), while significant innervation of the limb (HL) has occurred in heterozygous littermates (arrow 2). Other projections within the hindlimb are also reduced (arrows 3 and 4).

(G–J) E12.5 neurofilament labeling of cutaneous projections. (G and H) Cutaneous projections cover a greater portion of the skin in the hindlimb of *Magellan* mutants (arrows 1–3 are reference points for controls and mutants). (I and J) Higher magnification of (G) and (H) reveal defasciculation of sensory axons and smaller distal nerves (compare brackets).

Defining the behavior of individual motor axons is difficult when all axons are labeled. To asses the accuracy of motor axon navigation, we used the *SE1:GFP* reporter line which selectively labels the MMCm subset of motor neurons (medial motor column, median portion) that form the dorsal ramus (Shirasaki et al., 2006). Visualization of individual axons labeled with *SE1:GFP* revealed that MMCm cells turn toward their dorsal target without significant errors in their trajectory in control embryos (Figures 4C and 4E). Interestingly, *Magellan* mutant MMCm axons emerged from the spinal cord, but made numerous navigational corrections and often grew in the wrong direction over short distances (Figures 5D and 5F, arrows). One day later, at E11.5, misguided motor axons are observed within the DRG, and intense GFP labeling (which appeared as puncta at low magnification) is detected near the ventral root due to aberrant axon growth at the first choice point encountered in the periphery (Figures 5G and 5H).

Although these observations suggest that the misprojection phenotypes in *Magellan* mutants arise from wandering axons that do not properly respond to extracellular cues for axon navigation, we could not exclude the possibility that misprojections resulted from excess branching of individual axons. To test this, DiI backfills from the forelimbs were used. We reasoned that, if misprojections of motor neurons into the DRG were generated from interstitial axon branches, these projections would be labeled by backfilling motor nerves at the brachial plexus. Although these DiI fills labeled limb-innervating motor and sensory neurons as expected, there was no DiI labeling of the GFP^{+} motor axons within the DRG in *Magellan* mutants (Figures 5I–5K). Likewise, DiI fills from the limb failed to label axon branches entering the dorsal ramus. These findings suggest that axonal branching at proximal locations within embryos is not prevalent in *Phr1* mutants.

Normal Responses to Guidance Cues in *Magellan* Mutants

Signaling via Phr1 could regulate motor and sensory axon targeting through a number of potential mechanisms, such as (1) controlling neuronal cell fate or subtype diversification, (2) regulating the expression or function of axon guidance receptors, or (3) modulating the activity of signaling components downstream of guidance receptors. To investigate these possibilities, we first examined motor neuron differentiation through the use of markers for specific motor neuron subtypes: Hb9, Isl1, Lhx1 (Lim1), and Lhx3 (Lim3). This analysis revealed that the number and localization of motor neuron cell bodies and nuclei at ages from E10.5 to E12.5 were normal in *Magellan* mutant embryos (Figure S2, data not shown). The segregation of neurons into discrete motor columns also occurred normally in mutant mice, indicating that axon guidance errors within the periphery were not secondary to cell body migration errors.

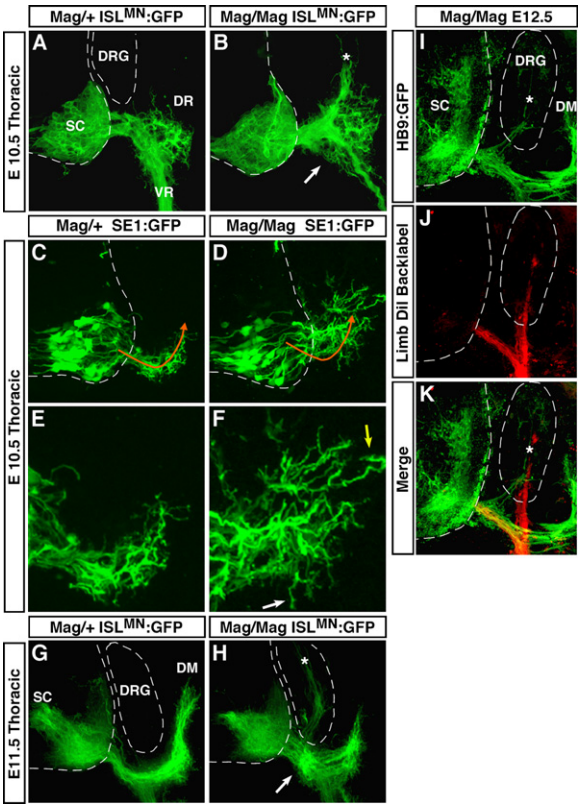

Figure 5. Motor Neuron Navigation Is Compromised in *Magellan* Embryos

(A) Transverse sections of control *ISL^{MN}:GFP* embryos at E10.5 reveals motor axons navigating through the dorsal ramus (DR)–ventral ramus (VR) choice point.

(B) In *Magellan* mutants, there is enhanced defasciculation around the choice point (arrow), the dorsal ramus is enlarged (asterisk), and the ventral ramus is smaller than normal.

(C–F) MMCm motor axon projections that form the dorsal ramus are selectively labeled with the *SE1:GFP* reporter. (C) At E10.5, MMCm axons begin to turn dorsally. (D) In *Magellan* mutants, MMCm motor axons fan out over a larger area. (E) High magnification of control in (C). (F) High magnification of (D) reveals MMCm axons that are extending in the wrong direction (wandering) in *Magellan* mutants (arrows).

(G and H) Transverse sections of *ISL^{MN}:GFP* E11.5 embryos. (G) Motor axons normally project to the dermomyotome (DM) or ventrally to the body wall. (H) In *Magellan* mutants, motor axons become disoriented within the choice point, leading to excessive growth and strong axon labeling at this site, creating the appearance of a GFP puncta (arrow) at low magnification. Axons that extend beyond the choice point occasionally enter the DRG inappropriately (asterisk).

(I–K) Interstitial branching of axons was monitored at E12.5 using retrograde DiI labeling from the forelimb of a *Magellan* mutant with *Hb9:GFP*-labeled motor neurons. (I) GFP labeling detects motor neuron misprojections within the DRG (asterisk). (J) DiI labeling of motor and sensory neurons. (K) The merge of (I) and (J) reveals that the GFP^{+} motor axons within the DRG are not DiI labeled (red) and therefore could not have formed as interstitial branches from limb-innervating motor neurons.

The axonal localization of Phr1 protein points toward a more direct role for this factor in pathfinding. The RING finger motif typical of E3-ubiquitin ligases on the C terminus of Phr1 may be involved in modulating guidance receptor protein levels and thereby influence the responsiveness of motor axons to guidance cues. For this reason, we analyzed the protein expression of a battery of known motor and sensory axon guidance receptors in *Magellan* mutants consisting of: EphA3, EphA4, ephrin-A5, cRet, cMet, Npn-1, TrkA, and TrkC (Figures 6A–6H, data not shown). At the level of sensitivity possible with immunohistochemistry, however, our "posttranslational regulation hypothesis" appeared to be incorrect because the level of protein expression of all tested guidance receptors in *Magellan* mutants was similar to the labeling in control embryos.

Next we considered the possibility that axon navigation defects in *Magellan* mutants arise from functional changes in guidance receptors or their downstream signaling components. To investigate this, we assayed the response of *Magellan* mutant axons to specific guidance cues using explant cultures. To test responses to attractants, motor explants from *Magellan* mutants and controls were cultured with EphA7-Fc to activate reverse signaling via ephrin-A5 receptors, or with BDNF to activate TrkB receptors. Attraction mediated by EphA7-Fc and outgrowth stimulation by soluble BDNF was similar from *Magellan* explants and controls (Figure 6J, data not shown). DRG explants were then tested for TrkA-mediated outgrowth in response to NGF. Without NGF, axons failed to grow from DRG-derived sensory explants in control experiments (data not shown), while addition of NGF elicited significant outgrowth of sensory axons (Figures 6M and 6N). To determine whether motor and sensory axon sensitivity to repulsive cues were altered, we quantified growth cone collapse in response to increasing concentrations of Sema3A-Fc and ephrin-A5-Fc, ligands for Npn1 and EphAs, respectively. Again we found that growth cones from *Magellan* mutant motor and sensory neurons responded with sensitivity similar to controls (Figure 6I, data not shown). Although these findings were contrary to our expectations, we found no evidence to suggest that either the expression of guidance receptors or functional responses to different types of guidance cues (i.e., contact-mediated, diffusible, attractive, repulsive) were measurably different in *Magellan* mutants.

The *Magellan* Mutation Alters Axon Morphology

Numerous axon guidance defects arise in *Magellan* mutants, yet we did not discover evidence that guidance cue responsiveness was altered. This prompted us to examine the growth behavior and morphology of individual axons to understand why axon guidance was defective in *Magellan* mutants. When grown on a permissive substrate containing laminin, mutant explants extended axons at a rate and length comparable to wild-type and heterozygous controls (Figures 6K–6N, data not shown). This suggested that the intrinsic machinery for axon growth was functional in *Magellan* mutants. However, wild-type motor axons grown in vitro typically extend in a single direction and rarely make large corrections in their

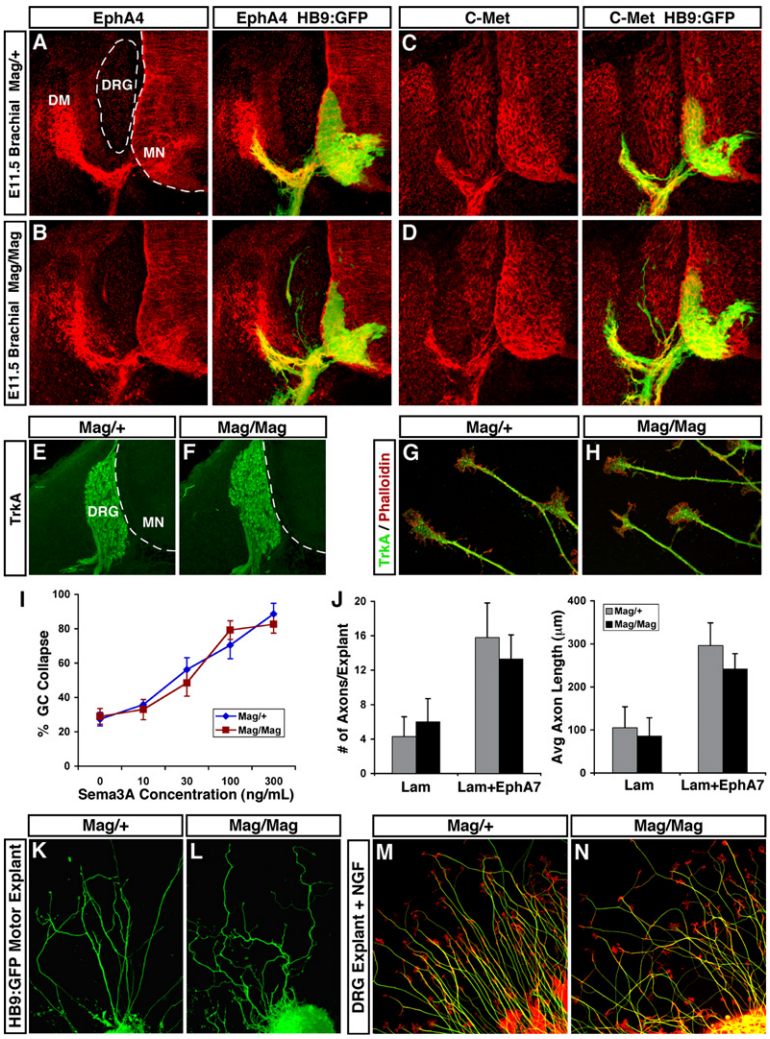

Figure 6. Axon Guidance Receptor Expression and Function Are Normal in *Magellan* Mutants

(A–D) Immunolabeling detects normal expression of EphA4 and C-Met in *Magellan* mutants.

(E–H) Expression of TrkA by sensory neurons is unchanged in *Magellan* mutants. (E and F) Transverse sections of E12.5 DRGs and (G and H) labeling of individual sensory growth cones detects normal TrkA expression (green) and phalloidin (F-actin, red).

(I and J) Quantification of motor neuron growth cone responses to guidance cues in culture. (I) Motor growth cone collapse in response to increasing concentrations of semaphorin occurred normally in *Magellan* mutants (red) as compared to heterozygous littermates (blue). (J) Increases in the number and length of motor axons in response to EphA7 (used as a ligand to promote reverse signaling via ephrin-As) was similar with mutants (black) and littermate controls (gray). Error bars were calculated as SEM.

(K and L) GFP$^+$ motor axons extend from explants dissected from *HB9:GFP* embryos. (K) Control. (L) The length of *Magellan* mutant motor axons was similar to wild-type, but displayed an abnormal kinked morphology.

(M and N) DRG sensory explants grown in the presence of NGF and labeled with Tuj1 (tubulin, green) and phalloidin (F-actin, red). Sensory axons extend normally from *Magellan* explants but turn more than controls.

trajectory greater than 15° in a 20 μm span. Mutant axons, in contrast, displayed an abnormal kinked morphology characterized by many turns over 15° (Figures 6K and 6L; Het = 0.8 kinks/axon, Mag = 3.7 kinks/axon). Sensory axons from DRG explants also displayed an abnormal growth pattern, although the turns were less abrupt, possibly due to the increased speed of sensory axon growth in culture (Figures 6M and 6N).

Growth Cones Are Abnormal in *Magellan* Mutants

To investigate how Phr1 regulates neuronal morphology, we monitored the outgrowth of sensory axons and the behavior of their growth cones in culture using time-lapse imaging. Normal growth cones maintain a highly polarized structure through a process in which F-actin containing filopodia protrude and then become engorged with microtubules, followed by local depolymerization of the F-actin within the neck of the growth cone, leading to "consolidation," whereby a stable axon is created from the trailing side of the extended growth cone (Aletta and Greene, 1988; Goldberg and Burmeister, 1986; Harris et al., 1987). During the course of our experiments with wild-type neurons, we observed these repeating stages involved in axon formation and separated this process into three phases: exploration (phase I), growth (phase II), and consolidation (phase III) (Figure 7A and Movie S1). Remarkably, *Magellan* mutant growth cones did not display these normal phases of outgrowth (Figure 7B and Movie S2). Instead, the axon shaft appeared to hyperextend into the growth cone so rapidly that the growth cone often failed to remain situated on the distal tip of the neurite, leading to the appearance of ectopic lamellipodia on the axon shaft. Often the ectopic growth cone-like structures were removed during the consolidation phase, and a new growth cone formed de novo at the tip of the neurite (Movies S2 and S3). Frequently, *Magellan* growth cones were abnormally bent in shape or had multiple axon shaft-like processes extend out of the growth cone, resulting in growth cone splitting (Figure 7H and Movie S4). Cultured motor neurons from *Magellan* mutants also exhibited defective growth cone morphologies, and the sites of sharp axon bends (kinks) appeared to correspond

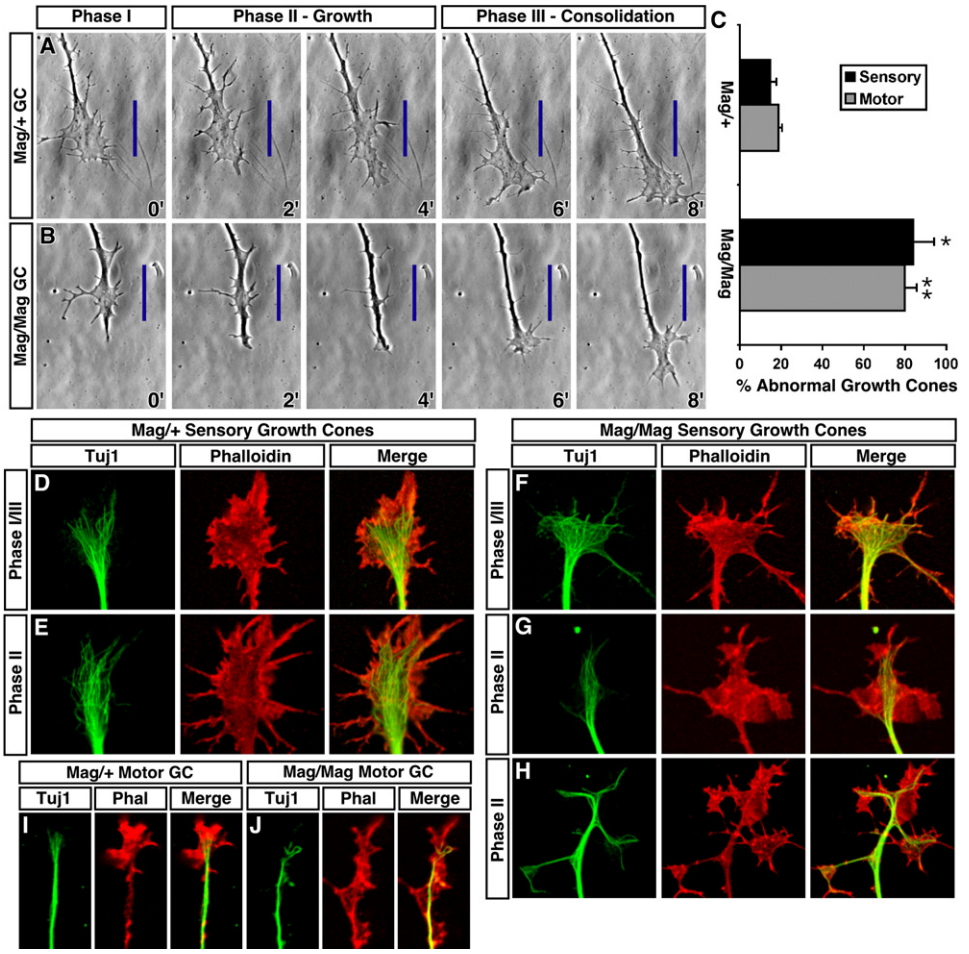

Figure 7. Growth Cone Morphology Is Altered in *Magellan* Mutants

(A and B) Time-lapse microscopy of sensory axons in culture. (A) Heterozygous control axons grow by extending growth cones (phase I and II), followed by the consolidation of the proximal growth cone segment into an axon shaft (phase III). Blue line provided as a reference point to more easily visualize axonal growth. (B) The axon shaft appears to extend past the growth cone during phase II in *Magellan* mutant axons, followed by slow elimination of growth cone material from the axon shaft and de novo regeneration of a growth cone on the tip of the axon.

(C) Quantification of the percentage of motor and sensory axons displaying abnormal growth cone morphology in culture. 79% ± 6% of mutant motor axons and 84% ± 9% of mutant sensory axons display growth cone defects, compared to 19% ± 3% and 15% ± 2% in control cultures. Error bars were calculated as SEM.

(D–H) Distribution of microtubules labeled with Tuj1 (green) and F-actin labeled with phalloidin (red) in actively extending sensory neuron growth cones. (D and E) Control growth cones at phase I/III and phase II. Microtubules (green) are within the axons and central region of the growth cone and are oriented in the direction of growth. (F and G) The microtubule cytoskeleton is highly abnormal in mutants. At phase I/III, the microtubules are disorganized and curved rather than exhibiting a biased orientation along the growth axis. In addition, the microtubules often extend beyond the central domain of the growth cone and enter into peripheral filopodial regions. (H) In many instances, the robust extension of microtubules into peripheral regions leads to split growth cones in *Magellan* mutants.

(I and J) The distribution of microtubules labeled with Tuj1 (green) and F-actin labeled with phalloidin (red) in motor neuron growth cones, which are significantly smaller than their sensory counterparts. (I) Control motor neurons have well-defined F-actin-rich growth cones on their neurite tips. (J) *Magellan* mutant motor neurons have abnormal F-actin-rich lamellipodial structures along their axon shafts.

to places where growth cone-like structures had become ectopically positioned on the shaft of motor axons (Figure S3).

To ascertain more precisely whether cytoskeletal defects underlie the *Magellan* phenotype, phalloidin staining was used to label filamentous F-actin in combination with immunolabeling for neuronal-tubulin (Tuj1). The typical polarized cytoskeletal organization within both motor and sensory growth cones was often highly abnormal in *Magellan* mutants (Figure 7C). During phase I/III, sensory growth cones from mutants were nearly filled with microtubules that were disorganized and not oriented in the direction of axon growth, unlike the ordered microtubule pattern seen with controls (Figures 7D and 7F). As *Magellan* mutant axons entered the growth phase (phase II), microtubules could be visualized abnormally extending

past the actin-rich growth cone, leaving ectopic actin patches along the axon shaft and no growth cone on the tip of the axon (Figures 7E and 7G). Likewise, ectopic F-actin patches were especially prominent on *Magellan* motor axons, as the microtubule cytoskeleton often overextended past the growth cone (Figures 7I and 7J). Taken together, these findings indicate that Phr1 is required to maintain the proper cytoskeletal polarization of growing neurons.

Phr1 Is Localized to Axon Shafts and Associates with the Microtubule Cytoskeleton

To understand how Phr1 regulates cytoskeletal dynamics within axons, its subaxonal localization was examined in motor explants. Phr1 labeling was found to be highest in the axonal segments of motor neurons, whereas growth cones and distal branches (which are often dynamic structures in culture) contained lower levels (Figure 8A). Similarly, Phr1 was most abundant within the axon shaft of sensory neurons grown as single-cell cultures and was undetectable in the growth cone (Figures 8F and 8H). Next we tested whether Phr1 is associated with the tubulin cytoskeleton within the axon using two independent methods. First, we performed a detergent extraction procedure on cultured motor explants that removes proteins not associated with the cytoskeleton (Ahmad et al., 1993). After extraction, cytosolic GFP (expressed from an *HB9:GFP* transgene) was eliminated as expected, while Phr1 was retained with axonal microtubules (Figures 8C and 8D). Second, we polymerized microtubules in vitro and monitored the fractionation of Phr1. E13.5 spinal cords were first homogenized, depolymerizing microtubules and leaving all tubulin in a monomeric soluble (S) form. GTP alone or GTP plus taxol was then added to this homogenate to promote microtubule repolymerization. Phr1 was found to associate with the microtubule pellet (P) fraction after polymerization, at levels comparable to the microtubule-associated protein MAP2 (Matus, 1994) (Figure 8E). As expected, the cytosolic protein GAPDH remained in the soluble fraction (Figure 8E). Taken together, these observations demonstrate that Phr1 associates either directly or indirectly with the microtubule cytoskeleton in growing axons. Unfortunately, in vitro experiments with purified proteins to assess whether Phr1 binds directly to microtubules were precluded due to difficulty in expressing adequate amounts of full-length Phr1, which is enormous.

Phr1 Regulates the Subcellular Localization of MAPKKK DLK

Genetic screens in invertebrates have identified functional interactions between *Phr1* orthologs *hiw/rpm-1* and the dual leucine zipper bearing MAP-kinase-kinase-kinases (MAPKKKs) *Wallenda* in *Drosophila* and *DLK-1* in *C. elegans* (Collins et al., 2006; Nakata et al., 2005). It is thought that the C-terminal ubiquitin ligase domain of *hiw/rpm-1* mediates the ubiquitination and proteasomal degradation of these MAPKKKs to regulate their activity. *Hiw/rpm-1* mutants display an accumulation of Wallenda/DLK-1 protein, and the increased MAPKKK levels are in turn thought to elevate P38 MAP kinase (P38MAPK) activity and thereby alter synaptic development (Collins et al., 2006; Nakata et al., 2005). To assess whether a similar Phr1-regulated pathway operates in mice to control axon navigation, we examined the expression of DLK, the closest mouse homolog to *Wallenda* and *DLK-1* (*Ensembl* database). Immunolabeling detected DLK protein in growing embryonic motor and sensory neurons, indicating that DLK was expressed in the same cell types as Phr1 (Figure S4). DLK labeling in cultured motor and sensory neurons revealed that it is enriched near the growth cone, with lower levels in the axon shaft (Figures 8B, 8G, and 8I). Since the distribution of DLK and Phr1 are inversely related (Figures 8F and 8G), we hypothesized that Phr1 may help to eliminate DLK from the axon shaft. Consistent with this idea, we observed an increase in DLK protein levels within the distal axons of *Magellan* mutants (Figures 8I and 8M), indicating that proper DLK compartmentalization is dependent on Phr1.

Examination of the junction between growth cones and axons revealed that Phr1 is present in the axon where stable acetylated tubulin is found, but is excluded from the central (core) domain of the growth cone where dynamic tyrosinated tubulin is present (Brown et al., 1993) (Figure 8J, data not shown). Conversely, DLK protein is present in puncta throughout the core and actin-rich peripheral domain of the growth cone with much lower levels in the distal axon shaft (Figure 8K). Similar localization patterns were present in motor growth cones, and the ectopic actin-rich patches that persist behind *Magellan* mutant motor growth cones contain high levels of DLK protein (Figures 8L and 8M). Taken together, these findings indicate that Phr1 is associated with stable microtubule structures within axons and helps to prevent DLK from accumulating in these regions.

The *Magellan* mutation results in expression of a truncated version of Phr1 that lacks ubiquitin ligase activity. To exclude the possibility that the truncated Phr1 protein had acquired neomorphic activity, we utilized siRNA-based knockdown of Phr1 expression in cultured sensory neurons to create a loss of function. Knockdown of Phr1 protein phenocopied the *Magellan* mutation, resulting in looped microtubules that filled the growth cone (Figures 9A–9C, compare to Figures 7D and 7F). Control siRNAs and nontransfected neurons in the culture did not display this phenotype (data not shown). These data indicate that the truncated Phr1 protein created by the *Magellan* mutation is inactive, as is the case with truncated forms of invertebrate *Phr1* orthologs (Wu et al., 2005).

Inhibiting P38MAPK or Increasing Microtubule Stability Reverses the *Magellan* Phenotype

The exclusion of DLK from stable portions of the axon shaft by Phr1, combined with the abnormal microtubule organization in the growth cones of *Magellan* mutants, suggested that the morphological defects were a byproduct of increased and/or ectopic MAP kinase signaling. If

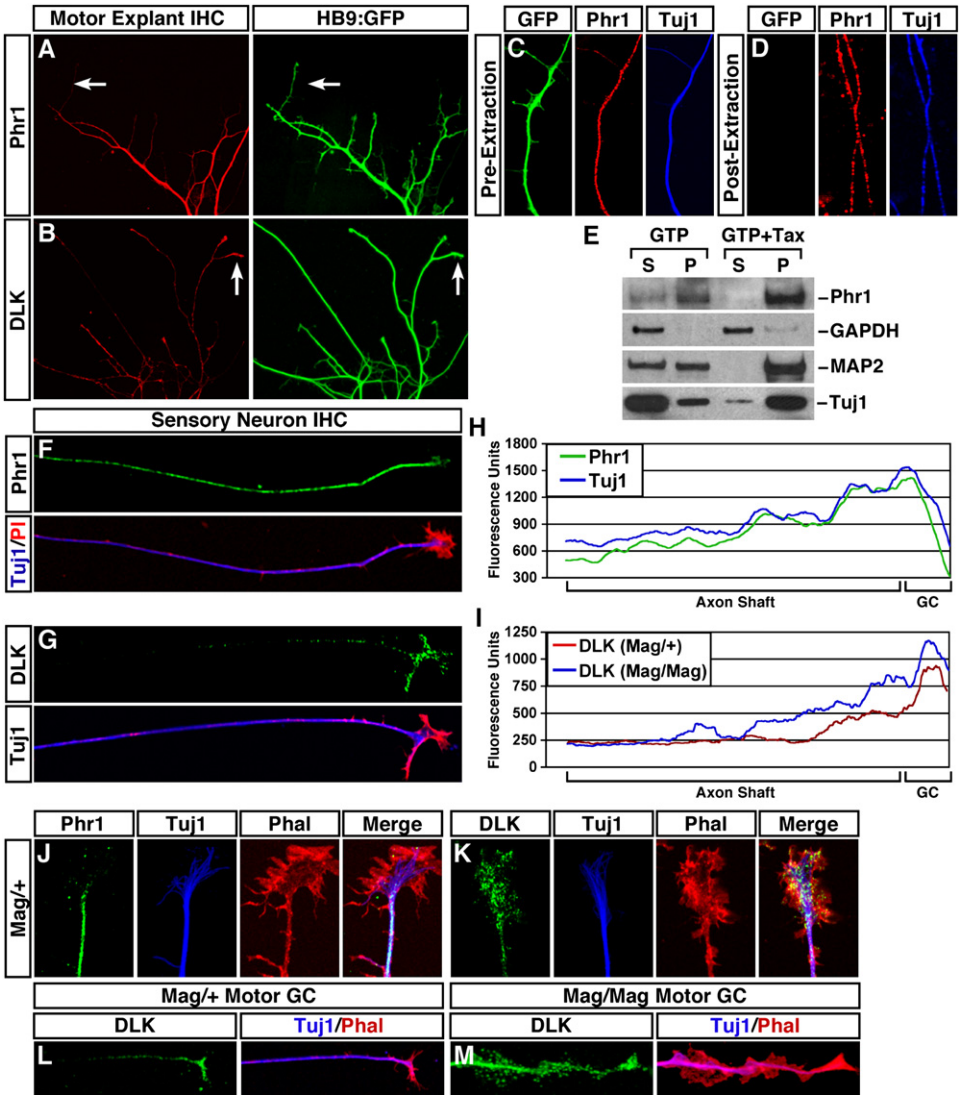

Figure 8. Subcellular Localization of Phr1 and DLK in Neurons

(A) *HB9:GFP*-labeled explants were cultured. Motor neuron processes are labeled with GFP. Phr1 protein is detected in the axon shaft, but is present at lower levels in newly formed collateral branches and growth cones (compare GFP and Phr1 labeling, arrows).

(B) Conversely, the highest levels of DLK protein occur within growth cones and distal branches.

(C and D) Cytosolic protein extraction from *HB9:GFP* motor axons grown in culture. Prior to extraction (C), high levels of cytosolic GFP are present. After extraction (D), cytosolic GFP is removed but Phr1 and tubulin (Tuj1) remain.

(E) Microtubule repolymerization assay with extracts from wild-type spinal cords incubated in the presence of GTP only or GTP plus 1 mM taxol to induce polymerization of monomeric tubulin. Soluble tubulin (S) polymerizes into microtubules, shifting into the pellet fraction (P) when GTP is added. Treatment with taxol enhances this effect. In both cases, Phr1 and the microtubule-associated control MAP2 are enriched in the pellet fraction, while the cytosolic control GAPDH remains soluble.

(F and G) Localization of Phr1 and DLK in cultured sensory neurons. In sensory neurons, Phr1 ([F], green) overlaps with tubulin (Tuj1, blue), but not F-actin in the growth cone (phalloidin, red). Conversely, DLK protein ([G], green) is more abundant in the F-actin (phalloidin, red) rich growth cone compared to the $Tuj1^{+}$ axon shaft (blue).

(H and I) Quantification of Phr1 and DLK localization using confocal line scans (see Experimental Procedures). In *Magellan* mutant neurons, DLK is detected at higher levels within the distal portion of the axon shaft and the growth cone.

(J and K) Distribution of Phr1 and DLK in sensory growth cones. (J) Phr1 is detected within the axon shaft but not the growth cone. (K) DLK concentrated in the growth cone region bordered by phalloidin labeling.

(L and M) Distribution of DLK in motor growth cones. In heterozygous controls, DLK ([L], green) expression is limited to the growth cone. In *Magellan* mutants, DLK ([M], green) spreads into the axon shaft and punctate staining is present in ectopic F-actin patches.

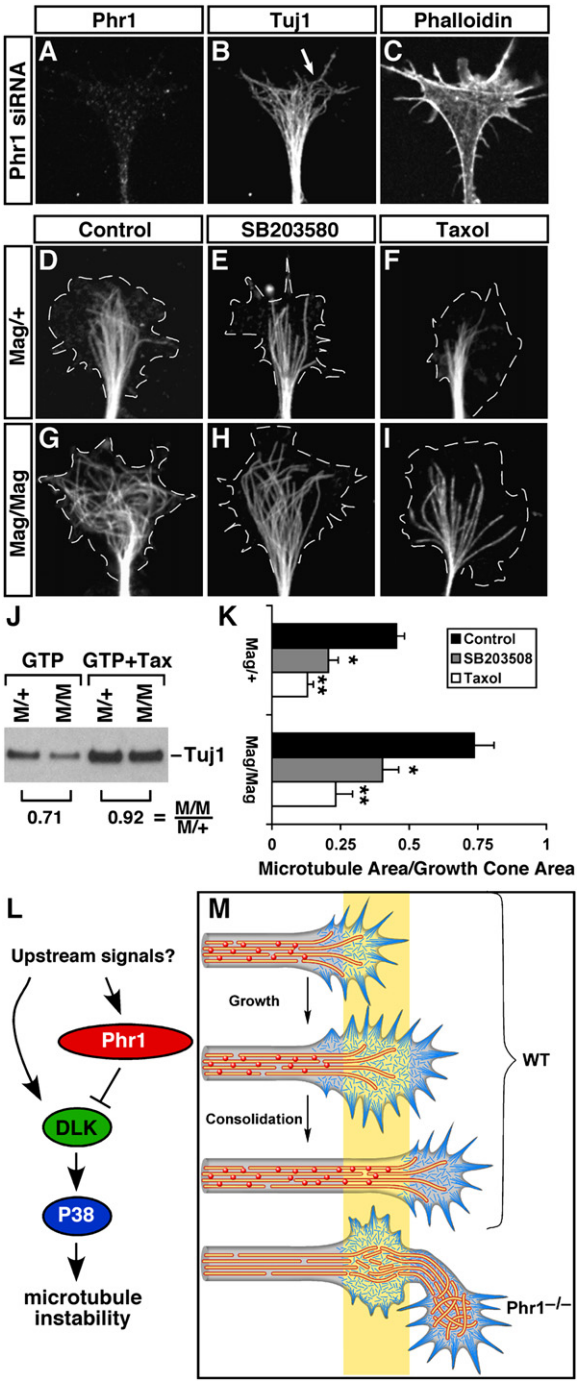

Figure 9. Microtubule Stabilization or Inhibition of P38MAPK Counteracts the Magellan Phenotype

(A–C) siRNA knockdown of Phr1 in sensory neuron cultures. Electroporation of *Phr1* siRNAs significantly decreased Phr1 protein levels (A) and induced disorganized, curved microtubules (B) that fill the F-actin-rich growth cone (C), similar to the phenotype observed *Magellan* mutants (compare to Figures 7D and 7F).

(D–I) Microtubule labeling (Tuj1) in sensory neurons. (D) Mock-treated control with normal microtubule organization. (E) P38MAPK inhibitor reduces microtubule formation. (F) Microtubule stabilization with taxol also reduces microtubule formation. (G) *Magellan* mutant sensory neurons have looped and disorganized microtubules. (H) Inhibition of P38MAPK restores the normal pattern of microtubules in *Magellan* mutants. (I) Likewise, treatment with taxol restores normal microtubules in the growth cones of *Magellan* mutant sensory neurons.

(J) Microtubule repolymerization assay. GTP alone or GTP plus taxol was added to spinal cord extracts containing an excess of monomeric soluble tubulin. Densitometry indicates that *Magellan* mutant extracts (M/M) treated with GTP have less tubulin in the microtubule pellet fraction than heterozygous controls (M/+) at steady state. The addition of taxol to the reaction shifted a higher fraction of tubulin into the pellet fraction in mutants.

(K) Quantification of images shown in (D)–(I). In each case, the ratio of growth cone area occupied by microtubules/total growth cone area was calculated. Heterozygous growth cones had ratios of 0.45 ± 0.02 for controls, 0.20 ± 0.03 for SB203580 treated, and 0.12 ± 0.03 for taxol treated, while mutant growth cones had ratios of 0.75 ± 0.06, 0.40 ± 0.06, and 0.23 ± 0.07. Data are representative of at least five growth cones in each condition. Error bars were calculated as SEM.

(L) Proposed signaling pathway for Phr1. Phr1 targets DLK directly or indirectly for degradation, thereby preventing it from generating signals that enhance microtubule instability. Thus, the presence of Phr1 in the axon shaft represents a negative regulator of a signaling pathway that favors dynamic cytoskeletal structures. Conversely, the lack of Phr1 in growth cones presumably allows the cytoskeleton to remain more dynamic in this region.

(M) Model for Phr1 function in axon navigation. The growth and consolidation stages of axon outgrowth are depicted, with an area of interest highlighted in yellow. Phr1 (red spheres) acts to stabilize microtubules in the axon shaft and ensure the growth cone remains on the tip of the axon. *Magellan* mutant axons (*Phr1*$^{-/-}$) do not consolidate the growth cone properly, which results in an excess of microtubules in the growth cone and F-actin-rich patches along the axon shaft.

this is indeed the case, inhibition of this kinase pathway should diminish the cytoskeletal defects associated with the *Magellan* mutation. As inhibitors of DLK do not exist, we tested a chemical inhibitor of P38MAPK, thought to function downstream of DLK. The P38 inhibitor SB203508 was added to the media of *Magellan* sensory explant cultures, and microtubule organization was analyzed. Remarkably, treatment with SB203508 eliminated the excess unpatterned microtubules that abnormally filled mutant growth cones (Figures 9D, 9E, 9G, 9H, and 9K). We next tested whether microtubule stability was altered in *Magellan* mutants by measuring the steady-state level of microtubule polymerization. Interestingly, extracts derived from *Magellan* mutants had reduced polymerized microtubule levels compared to controls in the presence of excess tubulin and GTP (Mag/control = 0.71 ± 0.08, Figure 9J). As expected, the addition of taxol shifted the equilibrium toward polymerization and increased microtubule levels with control and mutant extracts (Mag/control = 0.92 ± 0.06, Figure 8J). These observations suggested that the overly abundant and highly disorganized microtubule filaments within the growth cones of *Magellan* mutants arise due to an alteration of microtubule dynamics that enhances the kinetics of microtubule growth. We therefore predicted that taxol-enhanced stabilization (see Figure 9J) might reverse the *Magellan* phenotype. Indeed, taxol markedly reduced the number and overfilling of microtubules in *Magellan* growth cones and eliminated the disorganization of microtubule filaments (Figures 9D,

9F, 9G, 9I, and 9K). Our findings suggest that Phr1 functions to stabilize microtubules within the axon and inhibit the formation of dynamic cytoskeletal structures such as those in growth cones (Figures 9L and 9M).

DISCUSSION

In this study, we utilized a forward genetic screen in mice with GFP-labeled motor axons to identify molecules involved in neuronal pathfinding. We identified six recessive alleles and mapped the *Magellan* mutation to the *Phr1* gene. This gene encodes a large multidomain E3-ubiquitin ligase whose orthologs have previously been implicated in controlling synapse formation (Schaefer et al., 2000; Wan et al., 2000; Zhen et al., 2000). Three lines of evidence suggest that Phr1 is required cell-autonomously for proper axon growth: (1) it is not expressed by peripheral cells encountered by motor and sensory neurons when pathfinding, (2) individual *Magellan* mutant neurons cultured in isolation exhibit morphological defects, and (3) treatment of neuronal cultures with siRNA to knock down Phr1 lead to morphological defects only in the transfected cell population. In the future, targeted deletion of the *Phr1* gene using Cre-based strategies will help to precisely define the cell types that directly require Phr1 function. Phr1 associates with microtubules preferentially within the shaft of axons when neurons are actively navigating. In *Magellan* mutants, the loss of Phr1 function results in growth cone-like structures forming ectopically along sensory and motor axon shafts. Below we discuss how Phr1 regulates the dynamic relationship between the cytoskeleton within the growth cone and the axon shaft and why this is required for accurate and efficient axon navigation.

Axon Navigation in *Magellan* Mutants

The axons of growing neurons encounter choice points that represent sites of spatially localized extracellular cues for navigation. The presence and concentration of these extracellular guidance cues must be monitored at a subcellular level by the growth cone so that proper turning and growth decisions can be made (Dent and Gertler, 2003). The axon guidance decisions of embryonic motor neurons have been well characterized, and therefore we monitored the projections of these cells in our genetic screen (Kania and Jessell, 2003; Landmesser, 1978; Lieberam et al., 2005; Shirasaki and Pfaff, 2002). Axons from *Magellan* mutant motor neurons grew into inappropriate tissues, such as the DRG, and exhibited an unusual wandering behavior that frequently led to the accumulation of axons at major choice points, such as the proximal site for ventral and dorsal ramus formation and at the base of the limb. Using molecular markers we found that motor neurons are generated in their correct numbers at appropriate times within the developing embryo, and retrograde labeling experiments ruled out the possibility that the misguided processes in the DRG were interstitial branches derived from otherwise properly targeted motor axons. These findings prompted us to test whether the responsiveness to known guidance factors had been altered in *Magellan* mutants. Contrary to our expectations, however, cultured *Phr1* mutant neurons exhibited normal sensitivity to a variety of guidance signals.

In *Magellan* mutants, we found that motor as well as sensory neurons exhibited abnormal growth cone morphology, unusual axon growth behavior, and mislocalization of growth cone proteins. Normally, growth cones extend in three phases: protrusion of F-actin into filopodia, engorgement of filopodia with microtubules and organelles, and consolidation of the proximal region into a stable axon (Figure 9M) (Aletta and Greene, 1988; Goldberg and Burmeister, 1986; Harris et al., 1987). This sequential process ensures that the growth cone remains on the tip of the extending neurite and that its disto-proximal polarization is maintained, thereby ensuring that the leading edge of the neurite can rapidly reconfigure the cytoskeleton in response to guidance cues. Time-lapse imaging of *Phr1* mutant neurons revealed that the coordination between growth cone extension and axon consolidation had become decoupled. In many instances, the axon shaft pushed forward without properly maintaining the growth cone at the tip of the neurite, resulting in lamellipodial structures rich in F-actin accumulating along the proximal shaft of the axon. This abnormal growth behavior often resulted in growth cone splitting and/or the appearance of ectopic growth cones along the axon shafts of *Magellan* mutant neurons (Figure 9M). We speculate that although the signaling components for axon guidance are functional in *Magellan* mutants, the ineffective maintenance of growth cones on the distal ends of neurites in these mutants compromises their ability to precisely monitor the spatial distribution of guidance cues at choice points, leading to navigation errors and inappropriate axon turning that manifests itself as wandering and stalling in vivo.

Phr1-Based Signaling Regulates Microtubule Dynamics

Protein extraction from cells and microtubule polymerization studies in vitro independently showed that Phr1 is associated either directly or indirectly with microtubules. Furthermore, immunolabeling revealed that Phr1 is localized to the axon shaft of neurons where stable acetylated tubulin is concentrated, but it is absent from the core region of the growth cone where dynamic assembly and disassembly of tyrosinated microtubules occurs. Actin filament and microtubule assembly/disassembly play a vital role in growth cone motility during axon guidance, and there is a tight coordination between the formation of actin bundles and microtubule assembly (Suter et al., 2004; Williamson et al., 1996; Zhou and Cohan, 2004). Typically, microtubule ends within the core of the growth cone point in the forward direction, which contributes to the overall directionality of growth (Dent and Gertler, 2003; Gundersen and Bulinski, 1988). In addition, local stabilization of growth cone microtubules with taxol causes attractive

turning, whereas destabilization with noconazole repels neurons (Buck and Zheng, 2002). The signaling pathways that coordinate actin assembly with microtubule function are not well understood; however, a recent study has found that the actin-binding protein spinophilin influences microtubule bundling at the junction between growth cones and axons (Bielas et al., 2007).

In *Magellan* mutant neurons, we found that microtubule organization was abnormal. Disorganized microtubules filled a large portion of the growth cone and at times formed complete loops rather than orienting along the axis of neurite growth. Because Phr1 is localized to the axon shaft, the disorganized pattern of microtubules in *Magellan* growth cones presumably reflects a defect in the proper coordination between cytoskeleton assembly within the axon and the growth cone. Several observations suggest that microtubule turnover is more rapid in *Magellan* mutants. Polymerization studies found that the steady-state maintenance of tubulin within microtubules is reduced and that the microtubule stabilizer taxol restores the normal pattern of microtubule organization within the growth cone of *Magellan* mutant neurons. Although microtubule assembly is altered, the inherent ability of mutant neurons to extend axons was not affected. Nevertheless, *Phr1* mutants exhibited numerous directional changes (kinks) in their axons as opposed to the relatively straight growth observed in controls (Figure 9M).

The Phr1 Signaling Pathway

We found that the mitogen-activated protein kinase-kinase-kinase DLK and Phr1 are coexpressed by embryonic neurons, but they are localized in nonoverlapping cell compartments—DLK is found within growth cones, whereas Phr1 is in axons. Genetic elimination of invertebrate DLK orthologs has been shown to suppress the synaptic phenotypes that arise from mutations in *hiw* and *rpm1* (Collins et al., 2006; Nakata et al., 2005). These findings have led to a model in which the RING finger/E3-ubiquitin ligase activity of Phr1 targets DLK for proteosomal degradation. In support of this, we found that DLK became mislocalized in *Magellan* mutants, spreading into the axon shaft. Is enhanced DLK signaling linked to the morphological defects in *Magellan* mutant neurons? We examined this using an inhibitor of P38MAPK, a downstream protein activated by DLK. Similar to treatment with taxol, we found that suppressing P38 activity with SB203580 restored normal microtubule organization in *Phr1* mutant neurons. From these observations, we propose that Phr1 targets DLK for degradation in the axon, thereby excluding it from areas where stable microtubules are required. In contrast, the lack of Phr1 within growth cones should allow DLK to accumulate in this compartment of the neuron and modulate microtubule assembly via P38 (Figure 9L). Thus, a prediction from this model is that protein degradation regulates cytoskeletal organization. This hypothesis is strengthened further by the observation that proteasome inhibitors have been shown to disrupt the turning of retinal axons toward chemoattractants (Campbell and Holt, 2003).

Phr1: A Regulator of Axon Navigation, Axon Branching, and Synapse Formation

Phr1 orthologs have been identified in *C. elegans* (*rpm-1*), *Drosophila* (*hiw*), and zebrafish (*esrom*) (D'Souza et al., 2005; Schaefer et al., 2000; Wan et al., 2000; Zhen et al., 2000). *C. elegans rpm-1* mutants form larger but less abundant boutons, whereas *Drosophila hiw* mutants exhibit excessive terminal branching and an increase in neuromuscular junctions. We have not examined synapse formation in the *Magellan* mutant, but the phenotype is likely to be similar to the mouse piebald deletion spanning the *Phr1* gene, which consisted of excessive muscle nerve sprouting (Burgess et al., 2004). In contrast, retinal axons in zebrafish *esrom* mutants were found to stall prior to their proper tectal target (D'Souza et al., 2005). These differences could reflect separate functions for Phr1 in each species. Alternatively, the developmental stage of analysis and the specific features of each neuronal population examined may have led to different observed phenotypes.

Growth cone turning, interstitial branching, and synapse formation are thought to share similar cytoskeletal processes (Dent and Gertler, 2003; Kalil et al., 2000). How might Phr1 be involved in each process? In this report, we have shown that Phr1 is specifically localized to the axon shaft when neurons are pathfinding. Interstitial branches are thought to form along axon shafts where patches of F-actin accumulate, leading to the formation of growth cone-like structures (Kalil et al., 2000). Sites for interstitial axon branch formation might be unmasked by focal downregulation of Phr1 at specific locations along the axon shaft. In support of this, we have found that application of BDNF to *Magellan* mutant neurons leads to enhanced axonal branching (data not shown). Conversely, synapse formation requires the conversion of growth cones into stable terminal structures, which might occur if Phr1 localization is shifted to the distal end of the neuron when the target is encountered. In the future it will be interesting to determine whether the precise temporal and spatial regulation of Phr1 contributes to the alterations in cytoskeletal organization required at each of these stages of neuronal development.

EXPERIMENTAL PROCEDURES

Mice

The *ISL^{MN}:GFP-F* construct was generated by fusing the SE1 (crest1) element (Uemura et al., 2005) to a minimal CMV promoter to drive the expression of EGFP-F (BD Biosciences). EGFP-F was followed by a SV40 polyadenylation sequence and was flanked by 1.2 kb insulator sequences (West et al., 2002). *ISL^{MN}:GFP-F* mice were generated in a CB6 background and mated exclusively to C57/Bl6. *HB9:GFP* and *SE1:GFP* mice have been described (Lee et al., 2004; Shirasaki et al., 2006). Most mice used for experiments were backcrossed to C57/Bl6 mice for at least five generations, although *Magellan HB9:GFP* mice and *Magellan SE1:GFP* mice were kept in a mixed background.

ENU Screen

Fifty male DBA/2j mice (Jackson Labs) were given IP injections of 100 mg/kg ENU (Sigma) once a week for 3 consecutive weeks starting at 8 weeks of age. Eight to ten weeks after injection, animals regained fertility and were mated to *ISL^{MN}:GFP-F* mice. Eighty-eight GFP^{+} F1 males were generated and used in the screen. For each F1 "family," six to eight G3 litters containing at least four embryos each were examined. To screen embryos, mothers were sacrificed at 12.5 days postcoitum, and embryos were dissected and fixed for 2 hr in 4% paraformaldehyde in PBS. Embryos were transferred to PBS overnight and then decapitated, eviscerated, and cleared through a series of 30%, 50%, and 80% glycerol for 2 hr each. Cleared embryos were flattened between coverslips for visualization.

Mapping

A panel of 40 MIT markers was used for the initial mapping (Table S1), with three markers residing on chromosomes 1 and 2, and two markers on the other chromosomes. After the *Mag* mutation was localized to chromosome 14, additional SSLP and SNP markers were used to further refine the location of the mutation. MIT markers were selected based on a >10 bp difference between DBA and C57/Bl6 PCR products, and little to no difference between BALB/c and C57/Bl6 PCR products. To identify mutations in *Phr1*, overlapping 1 kb segments of the mRNA were amplified by RT-PCR from E12.5 whole-embryo RNA and sequenced.

Western Blotting, Immunohistochemistry, and In Situ Hybridization

Whole brains of E15 mice were dissected for western blots and sonicated in 500 μl RIPA buffer with protease inhibitors. Samples were run on a 3%–8% Tris-acetate gel (Invitrogen) and transferred according to the manufacturer's specifications, except that 0.05% SDS was added to the transfer buffer. Immunohistochemistry and in situ hybridization were carried out as described (Myers et al., 2005; Thaler et al., 2004). PAM (Phr1) antibody (PP3, V. Ramesh, Mass. General) was used at 1:100, DLK antibody (S. Ohno, Yokohama University) was used at 1:500. C-met (Santa Cruz), EphA4 (Santa Cruz), and TrkA antibodies were used at 1:1000. Whole-mount neurofilament staining was performed as described (Song et al., 2006). Microtubule repolymerization assays were performed as described (Gleeson et al., 1999), except that E13.5 spinal cords were used. The in situ probe for *Phr1* corresponds to nucleotides 1430–2325 of the coding sequence. For repolymerization assays measuring relative levels of pelleted microtubules in *Mag* mutants and controls, an excess of tubulin (cytoskeleton, Inc) was added to each reaction prior to incubation. All repolymerization assays are representative of at least three independent experiments. Errors were calculated based on (SEM), and significance was determined using the Mann-Whitney U test.

Imaging

Whole-mount images of *Isl^{MN}:GFP-F* mice were obtained using a 4× objective on a Olympus Fluoview 1000 confocal microscope. Close-up views of the whole-mount preparations and transverse sections depicting axon navigation are displayed as a flattened sum of multiple z-planes using a 10× objective. For Phr1 and DLK line scan intensity experiments, the fluorescence intensity was measured in 25 pixel steps along the length of the axon for five separate neurons and averaged.

Explant Cultures

Motor neurons were dissected from the spinal cords of E11.5–E12.5 mouse embryos in ice-cold Neurobasal medium. Explants were grown on coverslips that were coated with laminin (10 μg/ml for EphA7-Fc outgrowth, 100 μg/ml for other experiments) for >3 hr prior to culture and grown in neurobasal medium. Axons were allowed to grow for 24–36 hr and were then fixed with 4% paraformaldehyde in 5% sucrose. For sensory explants, DRGs from E13.5–E14.5 embryos were dissected and cultured on 10 μg/ml laminin for 20–24 hr in Neurobasal medium with 5% FBS (including 50 μg/ml NGF in most experiments). Explants were stained as above, except 0.5% Triton X-100 replaced Tween-20 in all buffers. Single-cell cultures were generated as described (Henderson et al., 1993) and grown in the medium above. Cytoskeletal extraction was performed as described previously (Ahmad et al., 1993). Prior to fixation, motor neuron explants were incubated with PEM buffer supplemented with 0.05% Triton X-100 and 10 μm taxol for 3 min. Cultures were then fixed and stained. Labeling of axons was performed using Alexa 568-conjugated phalloidin (Invitrogen) and antibodies against TuJ1 (Abcam, 1:2000). For siRNA experiments, three small RNAs corresponding to different regions of Phr1 (Invitrogen) were mixed and electroporated into DRG cultures using an Amaxa Nuclefocector device. For chemical inhibitor experiments, either 12.5 μM SB203508 (Calbiochem) or 20 nM taxol (Sigma) (both in DMSO) or DMSO alone were added at the start of the culture period. All explant and growth cone data presented are representative of at least five independent experiments for each condition. Errors were calculated based on (SEM), and significance was determined using the Mann-Whitney U test.

Supplemental Data

The Supplemental Data for this article can be found online at http://www.neuron.org/cgi/content/full/56/4/604/DC1/.

ACKNOWLEDGMENTS

We would like to thank Tamara Caspary and Kathryn Anderson for providing advice on the setup of the screen; Till Marquardt for assistance with motor explant cultures; Aaron DiAntonio and Suresh Jesuthasan for sharing unpublished results; and Joe Gleeson for advice on characterization of microtubules. We would also like to thank Vijaya Ramesh and Shigeo Ohno for generously providing antibodies to PAM and DLK, respectively. J.W.L is supported by a NRSA post-doctoral fellowship; N.G. is supported by the Swiss National Foundation; and this project was supported by NINDS.

Received: April 5, 2007
Revised: July 26, 2007
Accepted: September 11, 2007
Published: November 20, 2007

REFERENCES

Ahmad, F.J., Pienkowski, T.P., and Baas, P.W. (1993). Regional differences in microtubule dynamics in the axon. J. Neurosci. *13*, 856–866.

Aletta, J.M., and Greene, L.A. (1988). Growth cone configuration and advance: a time-lapse study using video-enhanced differential interference contrast microscopy. J. Neurosci. *8*, 1425–1435.

Bielas, S.L., Serneo, F.F., Chechlacz, M., Deerinck, T.J., Perkins, G.A., Allen, P.B., Ellisman, M.H., and Gleeson, J.G. (2007). Spinophilin facilitates dephosphorylation of doublecortin by PP1 to mediate microtubule bundling at the axonal wrist. Cell *129*, 579–591.

Briscoe, J., and Ericson, J. (2001). Specification of neuronal fates in the ventral neural tube. Curr. Opin. Neurobiol. *11*, 43–49.

Brown, A., Li, Y., Slaughter, T., and Black, M.M. (1993). Composite microtubules of the axon: quantitative analysis of tyrosinated and acetylated tubulin along individual axonal microtubules. J. Cell Sci. *104*, 339–352.

Buck, K.B., and Zheng, J.Q. (2002). Growth cone turning induced by direct local modification of microtubule dynamics. J. Neurosci. *22*, 9358–9367.

Burgess, R.W., Peterson, K.A., Johnson, M.J., Roix, J.J., Welsh, I.C., and O'Brien, T.P. (2004). Evidence for a conserved function in synapse

formation reveals Phr1 as a candidate gene for respiratory failure in newborn mice. Mol. Cell. Biol. *24*, 1096–1105.

Callahan, C.A., Muralidhar, M.G., Lundgren, S.E., Scully, A.L., and Thomas, J.B. (1995). Control of neuronal pathway selection by a Drosophila receptor protein-tyrosine kinase family member. Nature *376*, 171–174.

Campbell, D.S., and Holt, C.E. (2003). Apoptotic pathway and MAPKs differentially regulate chemotropic responses of retinal growth cones. Neuron *37*, 939–952.

Collins, C.A., Wairkar, Y.P., Johnson, S.L., and DiAntonio, A. (2006). Highwire restrains synaptic growth by attenuating a MAP kinase signal. Neuron *51*, 57–69.

Concepcion, D., Seburn, K.L., Wen, G., Frankel, W.N., and Hamilton, B.A. (2004). Mutation rate and predicted phenotypic target sizes in ethylnitrosourea-treated mice. Genetics *168*, 953–959.

D'Souza, J., Hendricks, M., Le Guyader, S., Subburaju, S., Grunewald, B., Scholich, K., and Jesuthasan, S. (2005). Formation of the retinotectal projection requires Esrom, an ortholog of PAM (protein associated with Myc). Development *132*, 247–256.

Dasen, J.S., Tice, B.C., Brenner-Morton, S., and Jessell, T.M. (2005). A Hox regulatory network establishes motor neuron pool identity and target-muscle connectivity. Cell *123*, 477–491.

Dent, E.W., and Gertler, F.B. (2003). Cytoskeletal dynamics and transport in growth cone motility and axon guidance. Neuron *40*, 209–227.

Dickson, B.J. (2002). Molecular mechanisms of axon guidance. Science *298*, 1959–1964.

Ebens, A., Brose, K., Leonardo, E.D., Hanson, M.G., Jr., Bladt, F., Birchmeier, C., Barres, B.A., and Tessier-Lavigne, M. (1996). Hepatocyte growth factor/scatter factor is an axonal chemoattractant and a neurotrophic factor for spinal motor neurons. Neuron *17*, 1157–1172.

Eberhart, J., Swartz, M.E., Koblar, S.A., Pasquale, E.B., and Krull, C.E. (2002). EphA4 constitutes a population-specific guidance cue for motor neurons. Dev. Biol. *247*, 89–101.

Finney, M., Ruvkun, G., and Horvitz, H.R. (1988). The C. elegans cell lineage and differentiation gene unc-86 encodes a protein with a homeodomain and extended similarity to transcription factors. Cell *55*, 757–769.

Gleeson, J.G., Lin, P.T., Flanagan, L.A., and Walsh, C.A. (1999). Doublecortin is a microtubule-associated protein and is expressed widely by migrating neurons. Neuron *23*, 257–271.

Goldberg, D.J., and Burmeister, D.W. (1986). Stages in axon formation: observations of growth of Aplysia axons in culture using video-enhanced contrast-differential interference contrast microscopy. J. Cell Biol. *103*, 1921–1931.

Gundersen, G.G., and Bulinski, J.C. (1988). Selective stabilization of microtubules oriented toward the direction of cell migration. Proc. Natl. Acad. Sci. USA *85*, 5946–5950.

Guo, Q., Xie, J., Dang, C.V., Liu, E.T., and Bishop, J.M. (1998). Identification of a large Myc-binding protein that contains RCC1-like repeats. Proc. Natl. Acad. Sci. USA *95*, 9172–9177.

Haase, G., Dessaud, E., Garces, A., de Bovis, B., Birling, M., Filippi, P., Schmalbruch, H., Arber, S., and deLapeyriere, O. (2002). GDNF acts through PEA3 to regulate cell body positioning and muscle innervation of specific motor neuron pools. Neuron *35*, 893–905.

Harris, W.A., Holt, C.E., and Bonhoeffer, F. (1987). Retinal axons with and without their somata, growing to and arborizing in the tectum of Xenopus embryos: a time-lapse video study of single fibres in vivo. Development *101*, 123–133.

Helmbacher, F., Schneider-Maunoury, S., Topilko, P., Tiret, L., and Charnay, P. (2000). Targeting of the EphA4 tyrosine kinase receptor affects dorsal/ventral pathfinding of limb motor axons. Development *127*, 3313–3324.

Helmbacher, F., Dessaud, E., Arber, S., deLapeyriere, O., Henderson, C.E., Klein, R., and Maina, F. (2003). Met signaling is required for recruitment of motor neurons to PEA3-positive motor pools. Neuron *39*, 767–777.

Henderson, C.E., Camu, W., Mettling, C., Gouin, A., Poulsen, K., Karihaloo, M., Rullamas, J., Evans, T., McMahon, S.B., Armanini, M.P., et al. (1993). Neurotrophins promote motor neuron survival and are present in embryonic limb bud. Nature *363*, 266–270.

Huber, A.B., Kania, A., Tran, T.S., Gu, C., De Marco Garcia, N., Lieberam, I., Johnson, D., Jessell, T.M., Ginty, D.D., and Kolodkin, A.L. (2005). Distinct roles for secreted semaphorin signaling in spinal motor axon guidance. Neuron *48*, 949–964.

Jessell, T.M., and Sanes, J.R. (2000). Development. The decade of the developing brain. Curr. Opin. Neurobiol. *10*, 599–611.

Kalil, K., Szebenyi, G., and Dent, E.W. (2000). Common mechanisms underlying growth cone guidance and axon branching. J. Neurobiol. *44*, 145–158.

Kania, A., and Jessell, T.M. (2003). Topographic motor projections in the limb imposed by LIM homeodomain protein regulation of ephrin-A:EphA interactions. Neuron *38*, 581–596.

Kasarskis, A., Manova, K., and Anderson, K.V. (1998). A phenotype-based screen for embryonic lethal mutations in the mouse. Proc. Natl. Acad. Sci. USA *95*, 7485–7490.

Kolodkin, A.L., Matthes, D.J., and Goodman, C.S. (1993). The semaphorin genes encode a family of transmembrane and secreted growth cone guidance molecules. Cell *75*, 1389–1399.

Kramer, E.R., Knott, L., Su, F., Dessaud, E., Krull, C.E., Helmbacher, F., and Klein, R. (2006). Cooperation between GDNF/Ret and ephrinA/EphA4 signals for motor-axon pathway selection in the limb. Neuron *50*, 35–47.

Landmesser, L. (1978). The development of motor projection patterns in the chick hind limb. J. Physiol. *284*, 391–414.

Landmesser, L.T. (1980). The generation of neuromuscular specificity. Annu. Rev. Neurosci. *3*, 279–302.

Lee, S.K., Jurata, L.W., Funahashi, J., Ruiz, E.C., and Pfaff, S.L. (2004). Analysis of embryonic motoneuron gene regulation: derepression of general activators function in concert with enhancer factors. Development *131*, 3295–3306.

Lieberam, I., Agalliu, D., Nagasawa, T., Ericson, J., and Jessell, T.M. (2005). A Cxcl12-CXCR4 chemokine signaling pathway defines the initial trajectory of mammalian motor axons. Neuron *47*, 667–679.

Marquardt, T., Shirasaki, R., Ghosh, S., Andrews, S.E., Carter, N., Hunter, T., and Pfaff, S.L. (2005). Coexpressed EphA receptors and ephrin-A ligands mediate opposing actions on growth cone navigation from distinct membrane domains. Cell *121*, 127–139.

Matus, A. (1994). Stiff microtubules and neuronal morphology. Trends Neurosci. *17*, 19–22.

McLaughlin, T., and O'Leary, D.D. (2005). Molecular gradients and development of retinotopic maps. Annu. Rev. Neurosci. *28*, 327–355.

Myers, C.P., Lewcock, J.W., Hanson, M.G., Gosgnach, S., Aimone, J.B., Gage, F.H., Lee, K.F., Landmesser, L.T., and Pfaff, S.L. (2005). Cholinergic input is required during embryonic development to mediate proper assembly of spinal locomotor circuits. Neuron *46*, 37–49.

Nakata, K., Abrams, B., Grill, B., Goncharov, A., Huang, X., Chisholm, A.D., and Jin, Y. (2005). Regulation of a DLK-1 and p38 MAP kinase pathway by the ubiquitin ligase RPM-1 is required for presynaptic development. Cell *120*, 407–420.

Novak, K.D., Prevette, D., Wang, S., Gould, T.W., and Oppenheim, R.W. (2000). Hepatocyte growth factor/scatter factor is a neurotrophic survival factor for lumbar but not for other somatic motoneurons in the chick embryo. J. Neurosci. *20*, 326–337.

Ozdinler, P.H., and Macklis, J.D. (2006). IGF-I specifically enhances axon outgrowth of corticospinal motor neurons. Nat. Neurosci. *9*, 1371–1381.

Santos, T.M., Han, S., Bowser, M., Sazani, K., Beauchamp, R.L., Murthy, V., Bhide, P.G., and Ramesh, V. (2006). Alternative splicing in protein associated with Myc (Pam) influences its binding to c-Myc. J. Neurosci. Res. *83*, 222–232.

Schaefer, A.M., Hadwiger, G.D., and Nonet, M.L. (2000). rpm-1, a conserved neuronal gene that regulates targeting and synaptogenesis in C. elegans. Neuron *26*, 345–356.

Sharma, K., Leonard, A.E., Lettieri, K., and Pfaff, S.L. (2000). Genetic and epigenetic mechanisms contribute to motor neuron pathfinding. Nature *406*, 515–519.

Shirasaki, R., and Pfaff, S.L. (2002). Transcriptional codes and the control of neuronal identity. Annu. Rev. Neurosci. *25*, 251–281.

Shirasaki, R., Lewcock, J.W., Lettieri, K., and Pfaff, S.L. (2006). FGF as a target-derived chemoattractant for developing motor axons genetically programmed by the LIM Code. Neuron *50*, 841–853.

Song, M.R., Shirasaki, R., Cai, C.L., Ruiz, E.C., Evans, S.M., Lee, S.K., and Pfaff, S.L. (2006). T-Box transcription factor Tbx20 regulates a genetic program for cranial motor neuron cell body migration. Development *133*, 4945–4955.

Suter, D.M., Schaefer, A.W., and Forscher, P. (2004). Microtubule dynamics are necessary for SRC family kinase-dependent growth cone steering. Curr. Biol. *14*, 1194–1199.

Tessier-Lavigne, M., and Goodman, C.S. (1996). The molecular biology of axon guidance. Science *274*, 1123–1133.

Thaler, J.P., Koo, S.J., Kania, A., Lettieri, K., Andrews, S., Cox, C., Jessell, T.M., and Pfaff, S.L. (2004). A postmitotic role for Isl-class LIM homeodomain proteins in the assignment of visceral spinal motor neuron identity. Neuron *41*, 337–350.

Uemura, O., Okada, Y., Ando, H., Guedj, M., Higashijima, S., Shimazaki, T., Chino, N., Okano, H., and Okamoto, H. (2005). Comparative functional genomics revealed conservation and diversification of three enhancers of the isl1 gene for motor and sensory neuron-specific expression. Dev. Biol. *278*, 587–606.

Van Vactor, D. (1998). Adhesion and signaling in axonal fasciculation. Curr. Opin. Neurobiol. *8*, 80–86.

Varela-Echavarria, A., Tucker, A., Puschel, A.W., and Guthrie, S. (1997). Motor axon subpopulations respond differentially to the chemorepellents netrin-1 and semaphorin D. Neuron *18*, 193–207.

Vrieseling, E., and Arber, S. (2006). Target-induced transcriptional control of dendritic patterning and connectivity in motor neurons by the ETS gene Pea3. Cell *127*, 1439–1452.

Wan, H.I., DiAntonio, A., Fetter, R.D., Bergstrom, K., Strauss, R., and Goodman, C.S. (2000). Highwire regulates synaptic growth in Drosophila. Neuron *26*, 313–329.

West, A.G., Gaszner, M., and Felsenfeld, G. (2002). Insulators: many functions, many mechanisms. Genes Dev. *16*, 271–288.

Williamson, T., Gordon-Weeks, P.R., Schachner, M., and Taylor, J. (1996). Microtubule reorganization is obligatory for growth cone turning. Proc. Natl. Acad. Sci. USA *93*, 15221–15226.

Wu, C., Wairkar, Y.P., Collins, C.A., and DiAntonio, A. (2005). Highwire function at the Drosophila neuromuscular junction: spatial, structural, and temporal requirements. J. Neurosci. *25*, 9557–9566.

Yamamoto, Y., Livet, J., Pollock, R.A., Garces, A., Arce, V., deLapeyriere, O., and Henderson, C.E. (1997). Hepatocyte growth factor (HGF/SF) is a muscle-derived survival factor for a subpopulation of embryonic motoneurons. Development *124*, 2903–2913.

Zallen, J.A., Yi, B.A., and Bargmann, C.I. (1998). The conserved immunoglobulin superfamily member SAX-3/Robo directs multiple aspects of axon guidance in C. elegans. Cell *92*, 217–227.

Zhen, M., Huang, X., Bamber, B., and Jin, Y. (2000). Regulation of presynaptic terminal organization by C. elegans RPM-1, a putative guanine nucleotide exchanger with a RING-H2 finger domain. Neuron *26*, 331–343.

Zhou, F.Q., and Cohan, C.S. (2004). How actin filaments and microtubules steer growth cones to their targets. J. Neurobiol. *58*, 84–91.